RXTE–PCA observations of XMMU J054134.7−682550

S. Ç. İnam,[1]★ L. J. Townsend,[2] V. A. McBride,[2] A. Baykal,[3]★ M. J. Coe[2]
and R. H. D. Corbet[4]

[1]*Department of Electrical and Electronics Engineering, Başkent University, 06530 Ankara, Turkey*
[2]*School of Physics and Astronomy, Southampton University, Hampshire SO17 1BJ*
[3]*Physics Department, Middle East Technical University, 06531 Ankara, Turkey*
[4]*University of Maryland, Baltimore County, Mail Code 662, NASA Goddard Space Flight Center, Greenbelt, MD 20771, USA*

ABSTRACT

We analysed *Rossi X-ray Timing Explorer* Proportional Counter Array observations of a recent outburst of the X-ray pulsar XMMU J054134.7−682550. We calculated the pulse frequency history of the source. We found no sign of a binary companion. The source spins up when the X-ray flux is higher, with a correlation between the spin-up rate and X-ray flux, which may be interpreted as a sign of an accretion disc. On the other hand, the source was found to have an almost constant spin frequency when the X-ray flux is lower without any clear sign of a spin-down episode. The decrease in pulsed fraction with decreasing X-ray flux was interpreted as a sign of accretion geometry change, but we did not find any evidence of a transition from accretor to propeller regimes. The source was found to have variable pulse profiles. Two peaks in pulse profiles were usually observed. We studied the X-ray spectral evolution of the source throughout the observation. Pulse-phase-resolved analysis does not provide any further evidence for a cyclotron line, but may suggest a slight variation of intensity and width of the 6.4 keV iron line with phase.

Key words: accretion, accretion discs – stars: neutron – pulsars: individual: XMMU J054134.7−682550 – X-rays: binaries.

1 INTRODUCTION

The X-ray pulsar XMMU J054134.7−682550 in the Large Magellanic Cloud (LMC) was discovered as a high-mass X-ray binary (HMXB) in an *XMM–Newton* survey of the LMC (Shtykovskiy & Gilfanov 2005). The source was then listed as a HMXB in a catalogue of HMXBs in the Magellanic Clouds (Liu, van Paradijs & van den Heuvel 2005).

From a routine scanning of *Swift*-Burst Alert Telescope (BAT) data on 2007 August 3, XMMU J054134.7−682550 was found to be in outburst with an increase in flux levels from ∼10–20 to ∼50 mCrab (Palmer, Grupe & Krimm 2007). Spectral features, the transient nature and pulsations at 61.6 s detected in *Rossi X-ray Timing Explorer* (*RXTE*) observations during the outburst were considered to be an indication of the HMXB nature of the source (Markwardt, Swank & Corbet 2007). These authors also noted the cyclotron absorption features at ∼10 and ∼20 keV in the X-ray spectrum of the source.

In this paper, we investigate the X-ray timing and spectral properties of the recent outburst of XMMU J054134.7−682550 from 2007

August 9 through 2007 November 1 (MJD 54321–MJD 54405). During this period, the 3–20 keV flux declined from ∼3.3 × 10⁻¹⁰ to ∼6 × 10⁻¹² erg s⁻¹ cm⁻². We track the changes in spin period of the source, relating these to the changes in the accretion geometry, and search for signatures of binarity in the light curve. We also study the evolution and flux dependence of the pulsed fraction through the outburst. Furthermore, we explore the spectral evolution of the source over the outburst and with neutron star spin phase, and investigate the possibility of cyclotron features in the spectrum.

2 INSTRUMENTS AND OBSERVATIONS

The Proportional Counter Array (PCA; Jahoda et al. 2006) on board the *RXTE* consists of five identical proportional counters coaligned to the same point in the sky, with a total geometric area of approximately 6250 cm^2, a field of view of 1 deg^2, and operating in the 2–60 keV energy range. In 2000 May and in 2006 December, PCU0 and PCU1, respectively, lost their propane veto layers. Without a propane veto layer, these PCUs have higher background levels. We have excluded the data from these PCUs in our spectral analysis. To obtain better energy channel counting statistics, we used only the data obtained from the top PCU layers for the spectral analysis. For both spectral and timing analyses, the latest combined

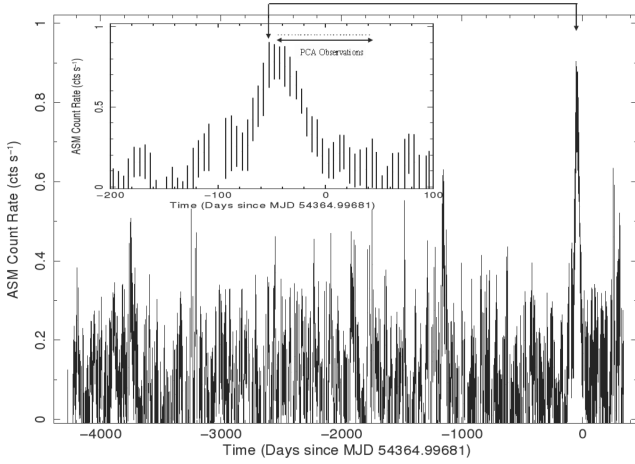★E-mail: inam@baskent.edu.tr (SÇİ); altan@astroa.physics.metu.edu.tr (AB)

Figure 1. Long-term *RXTE*–ASM light curve of XMMU J054134.7−682550. The inset shows a ∼300-day portion around the outburst at ∼MJD 54365. Dots in the inset represent individual PCA observations listed in Table 1.

background models were used together with HEASOFT 6.3 to estimate the appropriate background.

The long-term *RXTE*–All Sky Monitor (ASM) light curve of the source is presented in Fig. 1. *RXTE* observed XMMU J054134.7−682550 through a type II outburst, and 28 observations were undertaken between 2007 August 9 and 2007 November 1 with a total exposure of ∼127 ks (see Table 1). A 3–25 keV background-subtracted *RXTE* PCA light curve of the source is presented in Fig. 2. Although the number of active PCUs varied between one and three during the observations, count rates in Fig. 2 have been adjusted as if five PCUs were active using the CORRECTLC tool in HEASOFT.

3 TIMING ANALYSIS

We used background-corrected light curves for timing analysis. These light curves were also corrected to the barycentre of the Solar system. From the periodogram around 61 s, a period was found giving the maximum power. A template pulse profile from each *RXTE* observation was constructed by folding the data on this period. The template pulse profile comprising 20 phase bins was analytically represented by its Fourier harmonics (Deeter & Boynton 1985) and cross-correlated with the harmonic representation of average pulse profiles obtained from each observation. The maximum value of the cross-correlation is well defined and does not depend on the phase binning of the pulses. We used a 10-term unweighted harmonic series to cross-correlate the template pulse profile with the pulse profiles obtained from ∼400–500 s long segments of the observation. For each single or two succeeding *RXTE* observations, we obtained ∼5–12 arrival times. From the slopes of arrival times [$\delta\phi = \phi_0 + \delta\nu(t - t_0)$, where $\delta\phi$ is the pulse phase offset deduced from the pulse timing analysis, t_0 is the mid-time of the observation, ϕ_0 is the phase offset at t_0 and $\delta\nu$ is the deviation from the mean pulse frequency], we corrected the pulse frequencies which are presented in Fig. 3 (top panel).

We were able to phase connect all observation segments by using a fifth-degree polynomial in a Taylor expansion,

$$\delta\phi = \phi_0 + \delta\nu(t - t_0) + \frac{1}{2}\dot{\nu}(t - t_0)^2 + \frac{1}{6}\ddot{\nu}(t - t_0)^3$$
$$+ \frac{1}{24}\dddot{\nu}(t - t_0)^4 + \frac{1}{120}\ddddot{\nu}(t - t_0)^5, \tag{1}$$

Table 1. PCA observations of XMMU J054134.7−682550. The MJD column refers to the start of the observation.

Obs ID 93413-01-	Time (MJD)	Exposure (ks)
01-00	54321.108	3.5
03-00	54327.014	2.0
04-00	54330.669	1.4
04-01	54330.733	1.7
05-00	54333.796	3.9
06-00	54336.954	2.5
07-00	54339.707	3.2
08-01	54341.875	2.1
08-00	54342.197	0.9
09-00	54345.526	1.4
09-01	54345.798	2.0
10-00	54348.613	1.4
10-01	54348.678	1.6
11-00	54351.595	3.8
12-00	54354.950	5.5
13-00	54357.048	3.1
14-00	54360.133	1.8
15-00	54363.926	3.1
16-00	54366.932	2.9
17-00	54369.753	2.3
18-00	54372.491	1.4
18-01	54372.560	1.5
19-00	54375.628	2.6
20-00	54378.914	1.6
20-01	54379.121	1.4
21-00	54381.995	1.4
21-01	54382.06	1.5
22-00	54384.42	1.3
22-01	54384.474	1.6
23-00	54387.420	1.5
23-01	54387.486	1.5
24-00	54390.619	3.2
25-01	54393.519	1.5
25-00	54393.712	2.1
26-00	54396.704	3.5
27-00	54399.067	1.6
27-01	54399.143	2.5
28-00	54402.451	3.8
29-00	54405.807	2.2

where $\dot{\nu}$, $\ddot{\nu}$, $\dddot{\nu}$ and $\ddddot{\nu}$ are the first, second, third and fourth derivatives of the pulse frequency of the source. Pulse residuals from the subtraction of the fifth-degree polynomial are presented in Fig. 3.

Table 2 presents the timing solution of XMMU J054134.7−682550. In the top panel of Fig. 3, we present independent pulse frequency measurements for each observation and best-fitting model given by timing solution. In the middle and bottom panels, pulse frequency and pulse phase residuals are presented. In both residual panels, we have not seen any signature of a Doppler shift due to binary orbital modulation.

Folding 3–8, 8–13, 13–18 and 18–25 keV light curves of each observation with the pulse frequencies presented in Fig. 3, we obtained energy-dependent pulse profiles of the source. We present 12 sample pulse profiles from three observations in Fig. 4. We also obtained pulse profiles from 3–25 keV light curves. Using these pulse profiles, we calculated pulsed fractions using the definition $(F_{max} - F_{min})/(F_{max} + F_{min})$, where F_{max} and F_{min} are the highest and lowest fluxes of the phase bins. In Fig. 5, we present evolution and X-ray flux dependence of the pulsed fraction of the source.
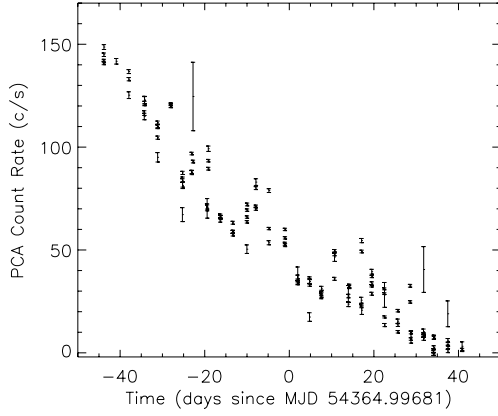
Figure 2. 61 s binned 3–25 keV light curve of XMMU J054134.7−682550.

X-ray flux values are obtained using the spectral analysis of the source (see next section).

For each sequence of three–four pulse frequency measurements, we fit a straight line to the pulse frequency time series in order to find the average pulse frequency derivatives. We plot the frequency derivative as a function of the average 3–20 keV X-ray flux in Fig. 6.

4 SPECTRAL ANALYSIS

Spectrum, background and response files for the observations were created using HEASOFT 6.3. We did not use channels corresponding to photon energies below 3 keV due to uncertainties in the background at these energies; neither did we use channels above 20 keV (25 keV for the brightest observation on MJD 54321) due to low count statistics. No systematic error was included in the fits, as statistical errors dominate for these data.

The brightest observation, on MJD 54321, was fit with an absorbed cut-off power law (White, Swank & Holt 1983), and a

Table 2. Timing solution of XMMU J054134.7−682550.

Parameter	Value
Epoch	MJD 54364.996 81(4)
Spin frequency(ν)	$1.645\,5121(7) \times 10^{-2}$ Hz
Spin frequency derivative ($\dot{\nu}$)	$3.1412(1) \times 10^{-11}$ Hz s^{-1}
$\ddot{\nu}$	$-1.2274(7) \times 10^{-17}$ Hz s^{-2}
$\dddot{\nu}$	$-1.25(8) \times 10^{-25}$ Hz s^{-3}
$\ddddot{\nu}$	$-8.0(1) \times 10^{-31}$ Hz s^{-4}
rms residual (pulse phase)	0.056

Gaussian emission component to account for a weak iron line at 6.4 keV. The neutral hydrogen density was unconstrained by the fit, and thus fixed to the line-of-sight value of 2.5×10^{21} cm^{-2} (Kalberla et al. 2005) . The fit, along with $\Delta \chi^2$ residuals, is shown in Fig. 7 and reported in Column 2 of Table 3.

Given that this model does not provide an optimal description of the observed spectrum ($\chi^2_\nu = 1.7$), and that Markwardt et al. (2007) reported possible cyclotron line features at 10 and 20 keV, we introduced cyclotron absorption features into the model at these energies. The model fit was clearly improved, however, the *F*-test probability of this improvement being by chance is quite significant: 0.018.

An alternative continuum model was then used (POWERLAW * HIGHECUT) which provided a better fit (see Table 3 and residuals in Fig. 7) of the continuum without the need for a cyclotron feature (see Fig. 7, lower panel). In this fit, we have allowed the neutral hydrogen density to vary, but it is still poorly constrained by the model. This model introduces a discontinuity in the spectrum at the cut-off energy, and such a discontinuity can disguise the presence of a cyclotron feature. Thus, our spectral analysis cannot confirm or rule out a cyclotron line in this source.

In order to investigate the variability of the spectrum through the outburst of XMMU J054134.7−682550, the best-fitting model
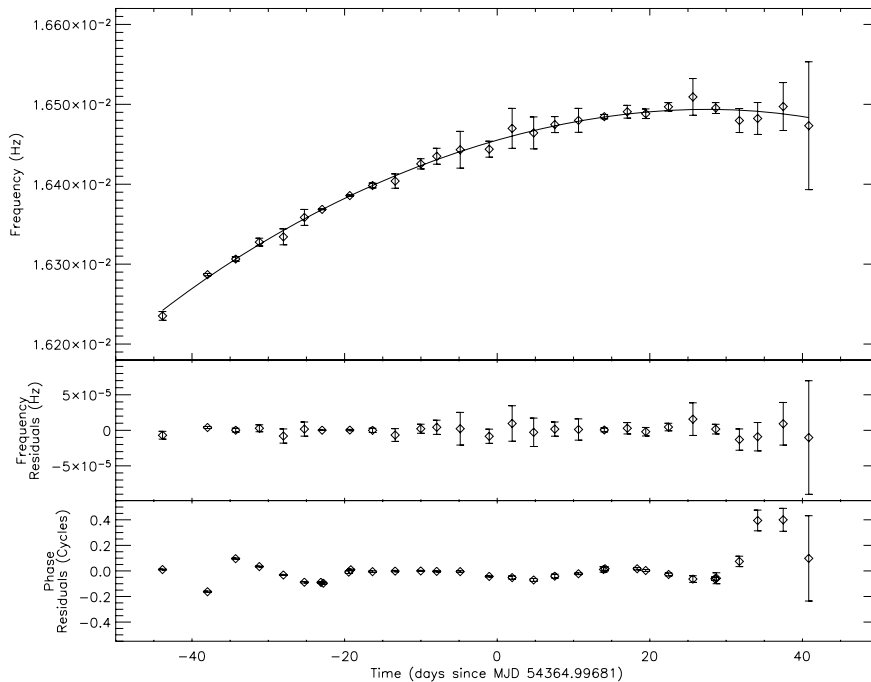
Figure 3. Pulse frequency and its best-fitting model (solid line), pulse frequency residuals and pulse phase residuals time series of XMMU J054134.7−682550. Each measurement corresponds to a single observation.
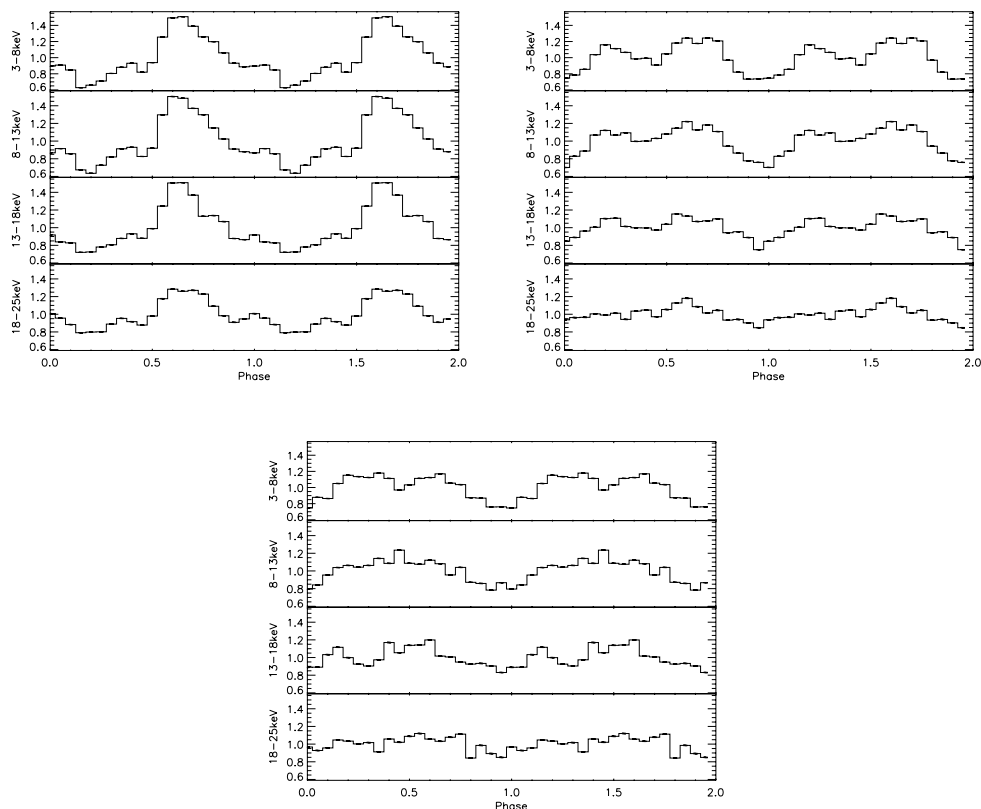
Figure 4. Energy-dependent pulse profiles for observations on MJD 54321.1 (top-left panel), MJD 54351.6 (top-right panel) and MJD 54387.4 (bottom panel). The unit of *y*-axis of each plot is normalized count from the specified energy interval.
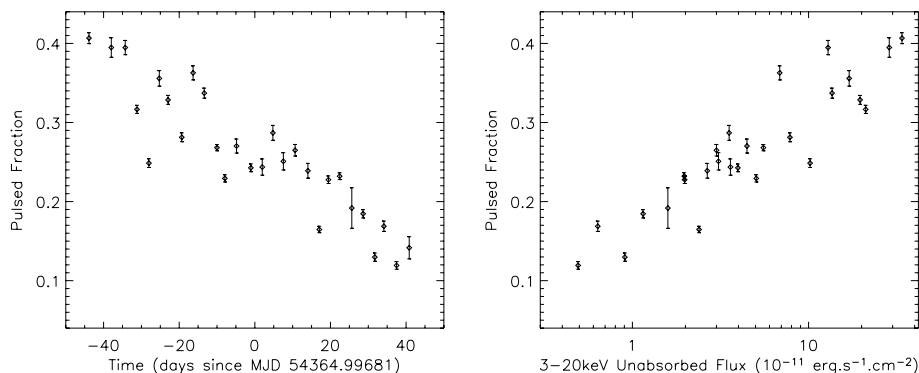

Figure 5. Evolution and X-ray flux dependence of pulsed fraction for XMMU J054134.7−682550.

above (POWER * HIGHECUT) was fit to all observations in Table 1 in 3–20 keV band using a fixed n_H value of 8×10^{20} cm^{-2}. For most observations, an Fe line at ∼6.4 keV was required to fit the spectra. From the spectral fits, cut-off energy values were found to be between ∼11 and ∼21 keV, and E_{fold} energy values were found to be between ∼4 and ∼33 keV. In Fig. 8, we plot 3–20 keV unabsorbed X-ray flux, spectral parameters and reduced χ^2 obtained from spectral fits as a function of observation days.

Assuming a distance of 49 kpc (Catalan & Cortes 2008) and using the unabsorbed X-ray flux values plotted in Fig. 8 and listed in Table 1, we found that X-ray luminosity of the source in the 3–20 keV band varies between ∼2×10^{36} and 9×10^{37} erg s^{-1}.

Fig. 9 shows the dependence of power-law index on the flux. The power-law index shows an anticorrelation with the flux, i.e. the spectrum gets softer with decreasing X-ray flux. Spectral softening

accompanied with X-ray flux decrease can be considered to be a result mass accretion rate variations (Meszaros et al. 1983; Harding et al. 1984), and is also observed in other accretion powered X-ray pulsars, like SAX J2103.5+4545 (Baykal, Stark & Swank 2002) and 2S 1417−62 (Inam et al. 2004).

5 PULSE-PHASE-RESOLVED SPECTROSCOPY

As cyclotron features are strongly dependent on viewing angle, phase-resolved spectroscopy was undertaken to further study the presence of possible cyclotron features. A secondary objective was to observe whether any other spectral features changed with the phase of the neutron star spin. Because of the distance to the source and the weakness of the possible cyclotron feature, we focus here on
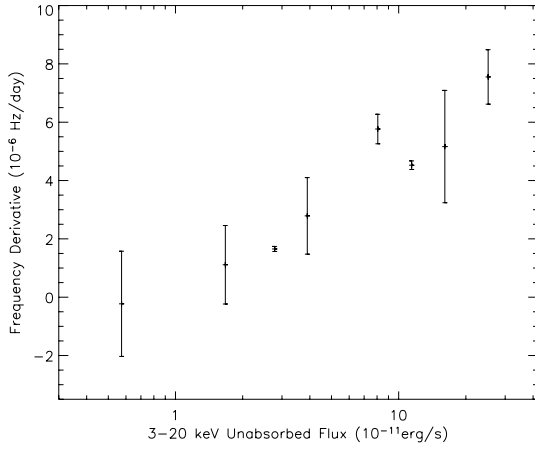
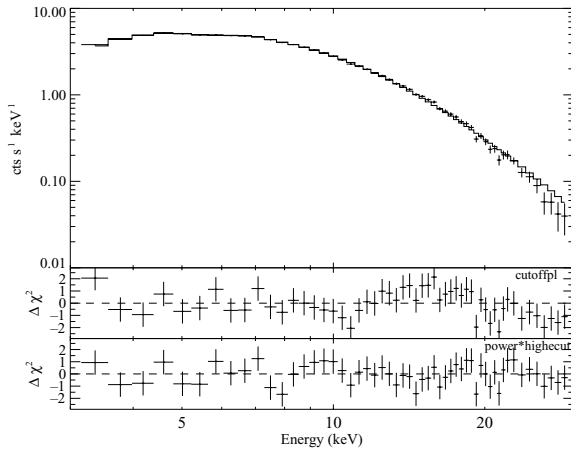**Figure 6.** Variation of frequency derivative with X-ray flux.

Figure 7. The upper panel shows the cut-off power-law model fitted to the spectrum. The middle panel shows the $\Delta\chi^2$ residuals from this model fit. A dip at around 10 keV is clearly shown, but the model is a poor fit to the continuum in general. The lower panel shows the $\Delta\chi^2$ residuals from fitting a power-law model with a high-energy cut-off. The dip at 10 keV is no longer apparent, showing that a cyclotron component at 10 keV is not necessary.

the brightest of the observations (01-00 at MJD 54321.1) to ensure the best signal-to-noise ratio possible.

The neutron star pulse period was arbitrarily divided into four phases according to the general morphology of the pulse profile, and in such a way that the chosen phases had broadly adequate signal-to-noise ratio. The upper panel of Fig. 10 shows the pulse profile for observation 01-00 folded on a 61.6 s period with the phase bins comprising two shoulder features and the rising and falling limbs of the main peak.

Using the spectral fits to the phase-averaged spectrum in the previous section as a guide, we fitted a cut-off power-law model to the phase-resolved spectra to see if there were any significant deviations from the phase-averaged continuum. The hydrogen column density was fixed to the standard LMC value of 2.5×10^{21} cm^{-2} (Kalberla et al. 2005). A simple absorbed cut-off power law was an adequate fit ($\chi^2_\nu < 1.1$) to the data for the Shoulder 1 and Main 1 phases, but an iron line at 6.4 keV (fixed) was required in the Main 2 and Shoulder 2 spectra. There was found to be little variation in the slope of the spectra, and all four showed weak signs of an absorption feature at 10 keV, much the same as the phase-averaged spectrum. In

Table 3. Results of spectral analysis. Errors are 90 per cent uncertainties. Flux is in erg cm^{-2} s^{-1}, and the Fe normalization in photons cm^{-2} s^{-1}.

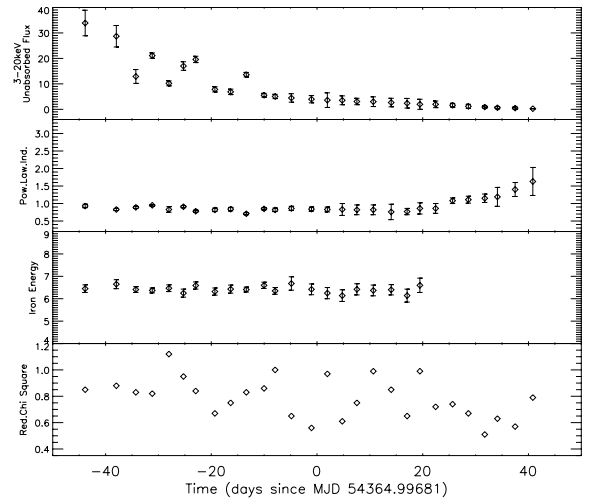| Parameter	CUT-OFFPL	POWER * HIGHECUT
$N_{\rm H} \times 10^{21}$ cm^{-2}	2.5 (fixed)	$0.8^{+0.8}_{-0.8}$
Γ	$0.42^{+0.05}_{-0.05}$	$0.95^{+0.05}_{-0.09}$
$E_{\rm cut}$ (keV)	–	$14.7^{+0.8}_{-0.8}$
$E_{\rm fold}$ (keV)	$14.3^{+0.5}_{-1.1}$	15^{+1}_{-1}
$E_{\rm Fe}$ (keV)	$6.5^{+0.2}_{-0.2}$	$6.5^{+0.3}_{-0.4}$
$\sigma_{\rm Fe}$ (keV)	$0.3^{+0.3}_{-0.3}$	$1.0^{+0.5}_{-0.4}$
Fe normalization	$2.4^{+0.9}_{-0.8} \times 10^{-4}$	$7^{+5}_{-3} \times 10^{-4}$
Unabsorbed flux (3–25 keV)	4.2×10^{-10}	4.2×10^{-10}
χ^2_ν (d.o.f.)	1.7 (50)	0.72 (48)

Figure 8. 3–20 keV unabsorbed flux in units of 10^{-11} erg s^{-1} cm^{-2}, power-law index, iron energy in units of keV and reduced χ^2 as a function of observation time. Errors indicate 1σ confidence level.
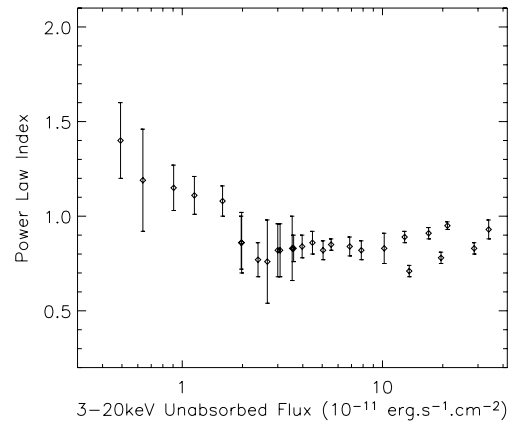

Figure 9. Variation of power-law index with X-ray flux.

the case of the Main 2 spectrum, however, the χ^2_ν was improved from 1.3 to 1.1 by the addition of a cyclotron feature at 10 keV. The F-test probability of this improvement being due to chance is 0.007, suggesting a rather marginal detection.

To be consistent with the analysis of the phase-averaged spectra, we also fitted an absorbed power-law model with a high-energy
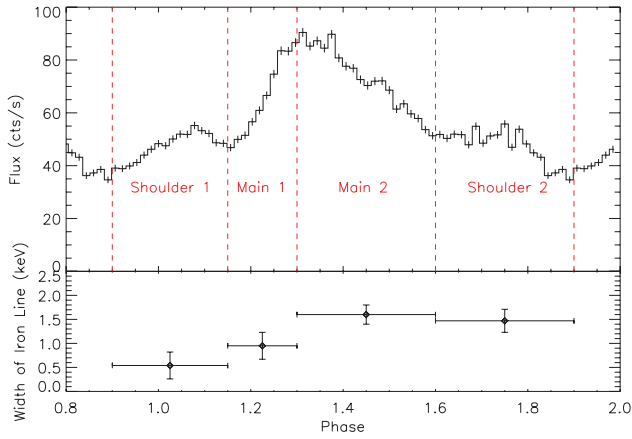
Figure 10. Upper panel: pulse profile for observation 01-00. The four phases studied are marked. Lower panel: width of iron line as a function of pulse phase using the power-law model with a high-energy cut-off. The y-errors are the 90 per cent uncertainties given by XSPEC.

cut-off. Again, this proved similar to the phase-averaged spectra in that the cut-off in the power law masked the residuals at 10 keV that were apparent in fitting the cut-off power law above. Once again, the hydrogen column density was fixed, and the energy of the iron line was fixed at 6.4 keV. With this model, too, the spectral slope showed little variation with pulse phase and no cyclotron features were required. Table 4 gives the parameters for the fits to the four spectra.

The lower panel of Fig. 10 shows the variation in the width of the iron line for the four phases of our pulse profile for the high-energy cut-off model with y-error bars the 90 per cent uncertainties from XSPEC. It is also clear from Table 4 that the iron line intensity follows the intensity of the source through the pulse profile, i.e. the iron line is strongest in the pulse peak. In Shoulder 1, the iron line is poorly constrained, and the low χ_ν^2, together with the errors on the line width, indicates that it is not strictly required in this phase. The errors are large due to the faintness of both the iron lines and are probably influenced by uncertainty in the underlying continuum. This makes it difficult to infer clearly any variation of the width of the line with phase from these data.

Neither of the models fitted points strongly towards the presence of a cyclotron feature in this source, however, given the quality of the data, a cyclotron line cannot be ruled out. The data suggest that there may be some variation in both the width and intensity of the 6.4 keV iron line through neutron star spin phase, but further observations below 3 keV, which will constrain the hydrogen column density, are required to show any such variation with certainty.

6 DISCUSSION AND CONCLUSION

The lack of orbital signature in pulse frequency and phase residuals is evident in Fig. 3. We also searched for a possible periodicity in the *RXTE*–ASM light curve as a sign of the binary orbit, but we did not find a sign of orbital modulation. The lack of orbital signature may be due to the fact that the orbital period of the binary system is larger than the total observation time-span of ~74 days. Future X-ray monitoring observations are needed to detect the signs of the orbit of this system.

The transient nature of the source may be a sign of a Be-type companion, i.e. the enhancement in the accretion rate may be due to the presence of a temporary accretion disc that forms when the neutron star enters denser equatorial stellar wind of the Be companion. Thus, the outburst is probably a type II outburst from a Be star system. From Fig. 1, this outburst is seen to be the brightest outburst from this source since the launch of *RXTE*.

In Fig. 3, a spin-up of trend of the source is evident especially for the first ~40 days of the observations. In Fig. 6, it is seen that flux is correlated with spin-up rate of the source. From Fig, 6, it is evident that observations corresponding to the lowest flux values have spin rates consistent with zero, showing that source is either spinning-up or it is at an almost constant spin frequency phase without any clear evidence of a spin-down episode. If we assume that observed X-ray luminosity is proportional to the bolometric luminosity (or mass accretion rate), then spin-up rate (which is proportional to torque exerted on the neutron star) and X-ray flux correlation can be explained by accretion from accretion discs when the net torque is positive and of the order of the material torque (Ghosh & Lamb 1979; Ghosh 1993). There are transient X-ray pulsar systems which show correlation between spin-up rate and X-ray flux: EXO 2030+375 (Parmar, White & Stella 1989; Wilson et al. 2002), A 0535+26 (Finger, Wilson & Harmon 1996a; Bildsten et al. 1997), 2S 1845−024 (Finger et al. 1999), GRO J1744−28 (Bildsten et al. 1997), GRO J1750−27 (Scott et al. 1997), XTE J1543+568 (in't Zand, Corbet & Marshall 2001) and SAX J2103.5+4545 (Baykal et al. 2002, 2007), 2S 1417−62 (Finger, Wilson & Chakrabarty 1996b; Inam et al. 2004). Thus, the positive correlation we show in Fig. 6 may be an indication of accretion via an accretion disc. However, without any orbital correction, it is not possible to analyse the nature of this correlation quantitatively, since the calculated pulse frequencies might not accurately correspond to the pulsar's spin frequencies.

Decreasing pulsed fraction with decreasing X-ray flux (Fig. 5) and changing pulse morphology (Fig. 4) may indicate changes in accretion geometry and even be an indicator of a transition from disc to wind accretion, or an ongoing transition from accretor phase to propeller phase. This is similar to the decrease in pulsed fraction and pulse morphology changes in the low X-ray flux observations in 2S 1417−62 (Inam et al. 2004). The evidence that observations

Table 4. Parameters from the power-law model with a high-energy cut-off fitted to the four phases indicated in Fig. 10. The centroid of the iron line was fixed at 6.4 keV and the N_H at 2.5×10^{21} cm^{-2} in all cases. Errors are 90 per cent uncertainties.

Parameter	Shoulder 1	Main 1	Main 2	Shoulder 2
σ_{Fe} (keV)	0.5 ± 0.3	1.0 ± 0.3	1.6 ± 0.2	1.5 ± 0.2
I_{Fe} (ph cm^{-2} s^{-1})	$(4 \pm 2) \times 10^{-4}$	$(9 \pm 4) \times 10^{-4}$	$(1.5 \pm 0.5) \times 10^{-3}$	$(9.1 \pm 0.5) \times 10^{-4}$
Γ	0.91 ± 0.02	0.86 ± 0.03	0.91 ± 0.01	0.90 ± 0.02
χ_ν^2 (58 d.o.f.)	0.69	0.81	0.92	1.10

corresponding to the lowest flux values have spin rates consistent with zero (Fig. 6) may also be an indicator of accretion geometry changes in the source.

The decline of the X-ray flux together with the change in pulse profile shapes and pulsed fraction may be an indication of a transition from accretor to propeller stage. When the propeller stage sets in, the great majority of accreting matter cannot reach the neutron star. To test this hypothesis, we can compare the factor of decrease in the bolometric luminosity with the theoretical expectation for accretion to propeller stage,

$$\Delta = 170 M_{1.4}^{1/3} R_6^{-1} P_0^{2/3}, \tag{2}$$

where $M_{1.4}$ is the mass of the neutron star in units of $1.4\,M_\odot$, R_6 is the radius of the neutron star in units of 10^6 cm and P_0 is the spin period of the neutron star in units of seconds (Corbet 1996; Campana & Stella 2000; Campana et al. 2002). The factor Δ becomes $\sim 2.6 \times 10^4$ for a neutron star with mass $\sim 1.4\,M_\odot$, radius $\sim 10^6$ cm and spin period of ~ 61 s. If we assume that the factor of decrease in bolometric luminosity is comparable to that of 3–20 keV luminosity, we find that our observed factor of luminosity change is ~ 50, which is much less than the theoretical expectation for a transition to propeller stage. It is not likely that we observe any transition to propeller stage.

As seen in Fig. 4, pulse profiles show high variability. Except 3–8, 8–13 and 13–18 keV pulse profiles of the observation on MJD 54321.1 and 18–25 keV pulse profile of the observation on MJD 54351.6, pulse profiles have two peaks separated by ~ 0.5 phase.

We found that both the phase-averaged spectrum could be fit with either a CUT-OFFPL model, with a possible weak cyclotron feature at 10 keV, or that it could be fit adequately using a power law with high-energy cut-off model without the need for a cyclotron feature. We used the power-law model with high-energy cut-off to map the spectral evolution throughout all observations (see Fig. 8).

We also constructed pulse-phase-resolved spectra from the brightest observation. From this analysis (see Fig. 10), we did not find any conclusive evidence of a cyclotron absorption feature, possibly due to low count statistics of the source. We found a very marginal variation in the iron line width and intensity which will need to be confirmed through further observations in the soft X-ray band.

ACKNOWLEDGMENTS

REFERENCES

Baykal A., Stark M., Swank J., 2002, ApJ, 569, 903
Baykal A., Inam S. C., Stark M. J., Heffner C. M., Erkoca A. E., Swank J. H., 2007, MNRAS, 374, 1108
Bildsten L. et al., 1997, ApJS, 113, 367
Campana L., Stella L., 2000, ApJ, 541, 849
Campana S., Stella L., Israel G. L., Moretti A., Parmar A. N., Orlandini M., 2002, ApJ, 580, 389
Corbet R. H. D., 1996, ApJ, 457, L31
Deeter J. E., Boynton P. E., 1985, in Hayakawa S., Nagase F., eds, Proc. Inuyama Workshop on Timing Studies of X-Ray Sources. Nagoya Univ., Nagoya, p. 29
Finger M. H., Wilson R. B., Harmon B. A., 1996a, ApJ, 459, 288
Finger M. H., Wilson R. B., Chakrabarty D., 1996b, A&AS, 120, 209
Finger M. H., Bildsten L., Chakrabarty D., Prince T. A., Scott D. M., Wilson C. A., Wilson R. B., Zhang S. N., 1999, ApJ, 517, 449
Ghosh P., 1993, in Holt S. S., Day C. S., eds, The Evolution of X-ray Binaries. Am. Inst. Phys., New York, p. 439
Ghosh P., Lamb F. K., 1979, ApJ, 234, 296
Harding A. K., Kirk J. G., Galloway D. J., Meszaros P., 1984, ApJ, 278, 369
Inam S. C., Baykal A., Scott D. M., Finger M., Swank J., 2004, MNRAS, 349, 173
in't Zand J. J. M., Corbet R. H. D., Marshall F. E., 2001, ApJ, 553, L165
Jahoda K., Markwardt C. B., Radeva Y., Rots A. H., Stark M. J., Swank J. H., Strohmayer T., Zhang W., 2006, ApJS, 163, 401
Kalberla P. M. W., Burton W. B., Hartmann D., Arnal E. M., Bajaja E., Morras R., Pöppel W. G. L., 2005, A&A, 440, 775
Liu Q. Z., van Paradijs J., van den Heuvel E. P. J., 2005, A&A, 442, 1135
Markwardt C. B., Swank J. H., Corbet R., 2007, Atel 1176
Meszaros P., Harding A. K., Kirk J. G., Galloway D. J., 1983, ApJ, 266, L33
Palmer D. M., Grupe D., Krimm H. A., 2007, Atel 1169
Parmar A. N., White N. E., Stella L., 1989, ApJ, 184, 271
Scott D. M., Finger M. H., Wilson R. B., Koh D. T., Prince T. A., Vaughan B. A., Chakrabarty D., 1997, ApJ, 488, 831
Shtykovskiy P., Gilfanov M., 2005, A&A, 431, 597
White N. E., Swank J. H., Holt S. S., 1983, ApJ, 270, 711
Wilson C. A., Finger M. H., Coe M. J., Laycock S., Fabregat J., 2002, ApJ, 570, 287

This paper has been typeset from a TEX/LATEX file prepared by the author.